

# A Comprehensive Analysis of Mamba for 3D Volumetric Medical Image Segmentation

Chaohan Wang<sup>a</sup>, Yutong Xie<sup>b,\*</sup>, Qi Chen<sup>a</sup>, Yuyin Zhou<sup>c</sup>, Qi Wu<sup>a</sup>

<sup>a</sup>*Australian Institute for Machine Learning, The University of Adelaide, Adelaide, Australia*

<sup>b</sup>*Computer Vision Department, MBZUAI, Abu Dhabi, United Arab Emirates*

<sup>c</sup>*Computer Science and Engineering Department, UC Santa Cruz, Santa Cruz, USA*

---

## Abstract

Mamba, with its selective State Space Models (SSMs), offers a more computationally efficient solution than Transformers for long-range dependency modeling. However, there is still a debate about its effectiveness in *high-resolution 3D medical image* segmentation. In this study, we present a comprehensive investigation into Mamba’s capabilities in 3D medical image segmentation by tackling three pivotal questions: Can Mamba replace Transformers? Can it elevate multi-scale representation learning? Is complex scanning necessary to unlock its full potential? We evaluate Mamba’s performance across three large public benchmarks—AMOS, TotalSegmentator, and BraTS. Our findings reveal that UlikeMamba, a U-shape Mamba-based network, consistently surpasses UlikeTrans, a U-shape Transformer-based network, particularly when enhanced with custom-designed 3D depthwise convolutions, boosting accuracy and computational efficiency. Further, our proposed multi-scale Mamba block demonstrates superior performance in capturing both fine-grained details and global context, especially in complex segmentation tasks, surpassing Transformer-based counterparts. We also critically assess complex scanning strategies, finding that simpler methods often suffice, while our Tri-scan approach delivers notable advantages in the most challenging scenarios. By integrating these advancements, we introduce a new network for 3D medical image segmentation, positioning Mamba as a transformative force that outperforms leading models such as nnUNet, CoTr, and U-Mamba, offering competitive accuracy with superior computational efficiency. This study provides key insights into Mamba’s unique advantages, paving the way for more efficient and accurate approaches to 3D medical imaging.

**Keywords:** Medical Image Segmentation, State Space Model, Transformer

---

## 1. Introduction

Volumetric medical image segmentation, which involves extracting 3D regions like organs, lesions, and tissues from modalities such as CT and MRI scans, is crucial for clinical applications like lesion contouring, diagnosis, and surgical planning. These tasks require not only local feature extraction but also the ability to capture long-range dependencies across entire volumes,

---

\*Corresponding author: Yutong Xie (e-mail: yutong.xie678@gmail.com).

which is vital for understanding the relationships between distant anatomical structures. Convolutional neural networks (CNNs), especially U-Net [1], are widely adopted for 3D medical image segmentation. Unet++ [2] enhances the U-Net by introducing nested and dense skip connections, while nnu-net [3] automates model design, training, and adaptation with minimal manual effort. However, the inherent limited receptive fields and locality biases of CNNs act as obstacles for capturing global context effectively. Transformers [4] models the long-range dependencies with dynamic self-attention mechanisms, but the computational complexity is impractical for handling large-scale, high-resolution 3D data.

With the introduction of the selective State Space Models (SSMs), Mamba [5] offers a promising alternative for modeling long-range dependencies in 3D medical image segmentation. Unlike Transformers, Mamba achieves higher inference throughput and scales linearly with sequence length, making it a more computationally efficient solution. This efficiency makes Mamba particularly well-suited for the demands of 3D medical imaging, where high-resolution volumetric data requires both precision and speed to process large-scale structures effectively. Inspired by Mamba’s recent success, a burgeoning body of work has sought to leverage its advantages for vision tasks. Pioneering efforts such as Vision Mamba (ViM) [6] and VMamba [7] employ multi-scan strategies, extending beyond vanilla Mamba’s single-scan approach, to effectively capture long-range dependencies in multiple directions. This enhancement significantly improves the model’s capability in modeling spatial relationships within complex image data. Several recent studies have specifically explored replacing Transformers with Mamba blocks in 3D medical image segmentation models. Notably, works like U-Mamba [8], SegMamba [9] and SwinUMamba [10] have successfully integrated Mamba blocks as plugins into convolutional neural network-based architectures, demonstrating promising results across various biomedical segmentation datasets. Within the broader field of pattern recognition, WtNGAN [11] has introduced Mamba to generative adversarial networks for unpaired image translation, underscoring Mamba’s versatility and emerging relevance beyond segmentation tasks. Nevertheless, existing research primarily demonstrates the feasibility of Mamba without fully investigating its broader capabilities or potential benefits in 3D medical image segmentation.

To address this gap, our work provides an in-depth analysis of Mamba’s impact by evaluating it on three challenging 3D medical image segmentation benchmarks, namely AMOS [12], TotalSegmentator [13], and BraTS [14]. The insights from these extensive evaluations offer a comprehensive understanding of Mamba’s applicability and set a foundation for future exploration. Our investigation focuses on three aspects:

**Mamba’s ability to replace Transformers** We aim to evaluate whether Mamba networks can replace Transformer-based architectures for long-range dependency modeling in 3D medical image segmentation, focusing on segmentation accuracy and computational efficiency. To this end, we designed two models: a Mamba-based network (UlikeMamba) and a Transformer-based network (UlikeTrans), both following a U-shaped encoder-decoder structure. Notably, we replace the original 1D depthwise convolutions (DWConv) [15] in Mamba with 3D DWConv to better preserve volumetric data’s spatial coherence. Our results show that UlikeMamba outperforms UlikeTrans in both accuracy and efficiency, especially with the 3D Mamba layer, while also avoiding the Out of Memory (OOM) issues faced by UlikeTrans.

**Mamba’s capacity to enhance multi-scale representation learning** This section delves deeper into Mamba’s potential for long-term dependency modeling to enhance multi-scale representation learning, a critical factor in achieving accurate 3D medical image segmentation. Successful volumetric segmentation requires the ability to capture both fine-grained details (such as small lesions or subtle tissue changes) and broader anatomical structures (such as large organs

like the liver, heart, or kidneys). We design and implement four distinct multi-scale modeling schemes, and our results show that Mamba-based models excel at capturing and integrating multi-scale features. These models consistently demonstrate superior performance, especially in complex tasks like TotalSegmentator, which involves segmenting 117 anatomical structures, proving Mamba to be a versatile and robust solution for challenging 3D medical image segmentation scenarios.

**Whether complex multi-way scanning strategies are necessary?** Mamba’s parallelized selective scan operation, designed for one-dimensional data, faces challenges when adapted to visual tasks. Many works, like Vision Mamba [6] and VMamba [7], introduce multi-way scanning mechanisms to preserve spatial coherence in vision tasks. To determine whether these complex scanning strategies are necessary for 3D medical image segmentation, we evaluate existing methods: single-scan (forward) and dual-scan (forward + backward) and introduce two new approaches: dual-scan (forward+random) and Tri-scan (left-right, up-down, front-back). Dual-scan (forward + backward) offers minimal improvement due to strong structural priors in medical data. While dual-scan (forward+random) may capture complex dependencies, it risks distorting these priors, compromising segmentation precision. Tri-scan delivers the best performance by preserving comprehensive spatial relationships but incurs higher computational costs. Simpler scanning methods often suffice, with Tri-scan proving advantageous in more complex scenarios.

Our contributions are three-fold:

1. Rather than simply designing a new network, we conduct a thorough analysis of Mamba’s role in 3D medical image segmentation, tailored to the specific challenges of the task, using three large, authoritative public datasets. This analysis provides strong insights and a foundation for future research in this domain.
2. We not only validate the effectiveness of existing strategies but also propose task-specific approaches, such as introducing 3D DWConv before SSM, developing multi-scale Mamba, and designing Tri-scan for 3D data, to further explore and enhance Mamba’s capabilities for volumetric medical image segmentation.
3. Using validated strategies, we construct a Mamba-based network that sets a new benchmark for 3D medical image segmentation, outperforming advanced models such as CNN-based nnUNet, Transformer-based CoTr, UNETR and SwinUNETR, as well as existing Mamba-based U-Mamba, offering competitive accuracy with higher computational efficiency.

## 2. Related Work

### 2.1. Transformer-based Segmentation Networks

Transformers have substantially influenced medical image segmentation through the powerful self-attention mechanism, enabling global context modeling across images. TransUNet [16] pioneered the integration of Transformers into U-Net architectures by coupling local CNN-based feature extraction with Transformer-based global dependency modeling, achieving superior segmentation accuracy. Subsequently, models like TransHRNet [17] tackled computational complexity through parallel multi-resolution strategies and Effective Transformer blocks, employing group linear transformations and spatial-reduction attention to balance efficiency and performance.

Further innovations include UCTNet [18], which selectively employs Transformers in uncertain regions identified via CNN-derived uncertainty maps, enhancing segmentation precision without significantly increasing computational burden. kMaXU [19] advances this hybrid approach by integrating CNN and Transformer encoders, addressing class imbalance with multi-scale k-Means Mask Transformer blocks, and improving consistency with cross-contrastive learning.

Collectively, these Transformer-based methods have significantly enhanced volumetric segmentation accuracy by capturing long-range dependencies. However, their high computational complexity remains challenging for large-scale, high-resolution 3D medical imaging. This motivates exploring alternative architectures, such as Mamba-based segmentation networks, which seek to maintain global context advantages while reducing computational overhead.

## 2.2. Mamba-based Segmentation Networks

Mamba [5], known for its ability to capture long-range dependencies with superior memory efficiency and computational speed compared to Transformers, has gained traction in medical image segmentation. In this domain, U-Net and its variants dominate, however, integrating Mamba with CNN architectures has sparked interest, leading to the development of both hybrid and pure Mamba-based models. These efforts aim to harness Mamba’s strengths in modeling global dependencies while maintaining the local feature extraction capabilities essential for segmentation.

In hybrid models, Mamba blocks are often combined with CNN-based architectures to balance the strengths of both methods. SegMamba [9] uses a multi-orientated Mamba module in the encoder, paired with CNN decoders. LKM-UNet [20] leverages large Mamba kernels and a hierarchical bidirectional Mamba block to improve local spatial modeling and efficient global dependency capture. Polyp-Mamba [21] enhances polyp segmentation by integrating multi-scale feature learning and semantic structure analysis, leveraging scale-aware semantics and global semantic injection to improve feature consistency and long-range interactions. H-vmunet [22] integrates High-order and Local 2D-selective-scan (SS2D) modules to improve global feature learning efficiency and local feature extraction. U-Mamba [8] combines Mamba and CNNs in both the encoder and decoder, offering improved global context comprehension. EM-Net [23] develops channel squeeze-reinforce Mamba (CSRm) blocks for selective attention and efficient frequency-domain learning (EFL) layers for learnable frequency weighting. Tri-Plane Mamba [24] introduces multi-scale 3D convolutional adapters and a tri-plane Mamba module to efficiently adapt Segment Anything Mode (SAM) for 3D medical image segmentation.

Pure Mamba-based models rely on Mamba blocks either in the encoder, combined with a CNN decoder, or throughout the entire architecture. VM-UNet [25] was the pioneering work to adopt this approach, using VSS blocks throughout. Swin-UMamba [10] replaces CNN blocks in the encoder with Visual State-Space (VSS) blocks, capturing contextual information and refining pixel- and patch-level features. UD-Mamba [26] presented a new pixel-level uncertainty-driven Mamba model to enhance medical image segmentation. Mamba-UNet [27] also employs a purely Mamba-based encoder-decoder structure with VMamba blocks in the bottleneck.

The developments demonstrate the versatility of Mamba in medical image segmentation, offering a range of solutions w.r.t. specific tasks. However, these initial works primarily validate the feasibility of Mamba in this domain, lacking a comprehensive analysis of its impact and potential advantages.

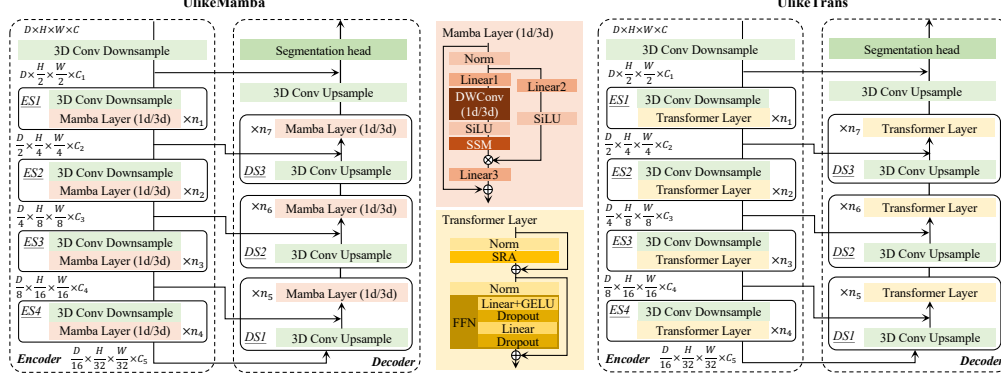


Figure 1: Mamba-based network (UlikeMamba) and Transformer-based network (UlikeTrans).

### 3. Material

We use three publicly available volumetric medical image segmentation datasets to comprehensively evaluate the performance. These datasets are widely recognized as benchmarks in the medical image analysis community, covering a broad range of anatomical regions and imaging conditions:

**AMOS dataset** [12] The AMOS dataset consists of 300 abdominal CT scans collected from multiple centers and vendors, encompassing various imaging modalities and phases. Each scan is annotated at the voxel level for 15 abdominal organs, presenting a challenging test-bed for segmentation algorithms. Its diversity in disease cases, patient demographics, and imaging conditions makes it ideal for studying model robustness in real-world scenarios. In our experiments, we used the official training and validation sets.

**TotalSegmentator (TotalSeg) dataset** [13] This dataset includes 1,228 CT images with annotations for 117 anatomical structures. The scans were randomly selected from clinical routines, offering a highly representative dataset that reflects real-world clinical conditions. The dataset spans a wide range of pathologies, scanners, sequences, and institutions, making it particularly well-suited for evaluating the generalizability of segmentation models. We used the official training and test sets in our experiments.

**BraTS 2021 challenge dataset** [14] The BraTS 2021 dataset includes 1,251 subjects, each with four 3D MRI modalities: native (T1), post-contrast T1-weighted (T1Gd), T2-weighted (T2), and T2 Fluid-attenuated Inversion Recovery (T2-FLAIR). It is a widely used benchmark for evaluating brain tumor segmentation algorithms, specifically for delineating tumor sub-regions such as enhancing tumor, necrosis, and edema, offering voxel-wise ground truth annotations provided by expert physicians. We split the dataset into 80% for training and 20% for testing.

### 4. Analysis 1: Mamba vs Transformer

#### 4.1. Experimental designs

This experiment is designed to compare the performance of U-shape Mamba- and Transformer-based networks, denoted as UlikeMamba and UlikeTrans, specifically for modeling long-range dependencies in volumetric medical image segmentation tasks. The goal is to

evaluate both segmentation accuracy and computational efficiency, which is crucial for practical applications in clinical environments. As shown in Fig. 1, both UlikeMamba and UlikeTrans consist of an encoder  $\mathcal{E}$  and a decoder  $\mathcal{D}$ . The corresponding blocks can be defined as

$$\begin{cases} \mathcal{E}_i := f_i \circ h_i & \mathcal{E}_i \in \mathcal{E} \\ \mathcal{D}_j := g_j \circ h_j & \mathcal{D}_j \in \mathcal{D}, \end{cases} \quad (1)$$

where  $f_i$  and  $h_i$  are the convolution layers and Mamba/Transformer layers, respectively, in the  $i$ -th block of the encoder, while  $g_j$  and  $h_j$  are the transposed convolution layers and Mamba/Transformer layers in the  $j$ -th block of the decoder. Concretely, in this section, we replace  $h$  from Transformer to Mamba while keeping others unchanged.

**Mamba-based network** As illustrated on the left of Fig. 1, the Mamba-based network, referred to as UlikeMamba, adopts a U-shaped encoder-decoder architecture [1]. The encoder consists of a 3D convolutional (Conv) block and four stages (ES1 to ES4), with each stage composed of a 3D Conv block followed by a Mamba layer. This progressively downsamples the input through 3D Conv blocks, generating feature embeddings at each stage, which are then flattened and passed into the Mamba layers for sequential processing. These Mamba layers balance computational efficiency and feature extraction across multiple resolutions. The Mamba layer processes input through a series of operations. First, the input is normalized and passed through a linear layer for initial feature transformation. Depthwise convolutions (DWConv) are then applied to capture local spatial features, followed by a SiLU activation function to introduce non-linearity. The data is further processed by the state space model (SSM), which efficiently captures long-range dependencies with linear complexity. A residual connection merges the output from the SSM with earlier features, followed by further refinement via a final linear layer.

The decoder structure mirrors the encoder and consists of three stages (DS1 to DS3). Each stage upsamples the feature maps using 3D transposed Conv layers, followed by Mamba layers to refine the upsampled features. Skip connections link corresponding encoder and decoder stages to retain high-resolution, low-level information essential for accurate segmentation. The final segmentation head outputs the segmentation map through a 3D Conv upsampling layer. This overall architecture leverages the Mamba’s strengths to efficiently process volumetric medical images while maintaining low computational overhead compared to more complex architectures. The specific architecture details can be found on the left of Fig. 2.

**Transformer-based network** The Transformer-based network, as shown on the right in Fig. 1, adopts a U-shaped encoder-decoder architecture similar to the Mamba-based network, but replaces the Mamba layers with Transformer layers, hence referred to as UlikeTrans. Each Transformer layer consists of a self-attention module and a feed-forward network (FFN) with two hidden layers. Initially, we experimented with vanilla point-to-point self-attention, however, this approach resulted in extreme computational complexity and excessive memory usage when applied to 3D volumetric images, making quantitative comparisons impractical. To address this, we implemented the spatial-reduction attention (SRA) layer [28] to reduce spatial complexity and enable UlikeTrans to handle high-resolution volumetric medical images for comparisons. Given a query  $q$ , a key  $k$ , and a value  $v$  as the input, SRA first reduces the spatial resolution of  $k$  and  $v$ , and then feeds  $q$ , reduced  $k$ , and reduces  $v$  to a multi-head self-attention layer to produce refined features. The specific architecture details can be found on the right of Fig. 2.

#### 4.2. Training setup and evaluation metrics

Both UlikeMamba and UlikeTrans were implemented using the nnUNet [3] framework, which automatically selects batch sizes and patch sizes tailored to each dataset. We utilized the AdamW

Layer_name		UlikeMamba_3d	Output Size
3D Conv Downsample		Conv: K=7, C=32, S=(1,2,2)	$D \times \frac{H}{2} \times \frac{W}{2}$
ES1	3D Conv Downsample	Conv: K=3, C=48, S=2	$\frac{D}{2} \times \frac{H}{2} \times \frac{W}{2}$
	Mamba Layer	$\begin{bmatrix} \text{Linear1: } 48 \rightarrow 2 \times 48 \\ \text{Linear2: } 48 \rightarrow 2 \times 48 \\ \text{DWConv: } K=3 \times 3 \times 3, C=2 \times 48 \\ \text{SSM, } C=2 \times 48 \\ \text{Multiplicative} \\ \text{Linear3: } 2 \times 48 \rightarrow 48 \end{bmatrix} \times 2$	$\frac{D}{2} \times \frac{H}{4} \times \frac{W}{4}$
ES2	3D Conv Downsample	Conv: K=3, C=128, S=2	$\frac{D}{4} \times \frac{H}{4} \times \frac{W}{8}$
	Mamba Layer	$\begin{bmatrix} \text{Linear1: } 128 \rightarrow 2 \times 128 \\ \text{Linear2: } 128 \rightarrow 2 \times 128 \\ \text{DWConv: } K=3 \times 3 \times 3, C=2 \times 128 \\ \text{SSM, } C=2 \times 128 \\ \text{Multiplicative} \\ \text{Linear3: } 2 \times 128 \rightarrow 128 \end{bmatrix} \times 3$	$\frac{D}{4} \times \frac{H}{8} \times \frac{W}{8}$
ES3	3D Conv Downsample	Conv: K=3, C=256, S=2	$\frac{D}{8} \times \frac{H}{16} \times \frac{W}{16}$
	Mamba Layer	$\begin{bmatrix} \text{Linear1: } 256 \rightarrow 2 \times 256 \\ \text{Linear2: } 256 \rightarrow 2 \times 256 \\ \text{DWConv: } K=3 \times 3 \times 3, C=2 \times 256 \\ \text{SSM, } C=2 \times 256 \\ \text{Multiplicative} \\ \text{Linear3: } 2 \times 256 \rightarrow 256 \end{bmatrix} \times 4$	$\frac{D}{8} \times \frac{H}{16} \times \frac{W}{16}$
ES4	3D Conv Downsample	Conv: K=3, C=512, S=2	$\frac{D}{16} \times \frac{H}{32} \times \frac{W}{32}$
	Mamba Layer	$\begin{bmatrix} \text{Linear1: } 512 \rightarrow 2 \times 512 \\ \text{Linear2: } 512 \rightarrow 2 \times 512 \\ \text{DWConv: } K=3 \times 3 \times 3, C=2 \times 512 \\ \text{SSM, } C=2 \times 512 \\ \text{Multiplicative} \\ \text{Linear3: } 2 \times 512 \rightarrow 512 \end{bmatrix} \times 3$	$\frac{D}{16} \times \frac{H}{32} \times \frac{W}{32}$
DS1	3D Conv Upsample	TransposeConv: K=2, C=256, S=2	$\frac{D}{8} \times \frac{H}{16} \times \frac{W}{16}$
	Mamba Layer	$\begin{bmatrix} \text{Linear1: } 256 \rightarrow 2 \times 256 \\ \text{Linear2: } 256 \rightarrow 2 \times 256 \\ \text{DWConv: } K=3 \times 3 \times 3, C=2 \times 256 \\ \text{SSM, } C=2 \times 256 \\ \text{Multiplicative} \\ \text{Linear3: } 2 \times 256 \rightarrow 256 \end{bmatrix} \times 3$	$\frac{D}{8} \times \frac{H}{16} \times \frac{W}{16}$
DS2	3D Conv Upsample	TransposeConv: K=2, C=128, S=2	$\frac{D}{4} \times \frac{H}{8} \times \frac{W}{8}$
	Mamba Layer	$\begin{bmatrix} \text{Linear1: } 128 \rightarrow 2 \times 128 \\ \text{Linear2: } 128 \rightarrow 2 \times 128 \\ \text{DWConv: } K=3 \times 3 \times 3, C=2 \times 128 \\ \text{SSM, } C=2 \times 128 \\ \text{Multiplicative} \\ \text{Linear3: } 2 \times 128 \rightarrow 128 \end{bmatrix} \times 4$	$\frac{D}{4} \times \frac{H}{8} \times \frac{W}{8}$
DS3	3D Conv Upsample	TransposeConv: K=2, C=48, S=2	$\frac{D}{2} \times \frac{H}{4} \times \frac{W}{4}$
	Mamba Layer	$\begin{bmatrix} \text{Linear1: } 48 \rightarrow 2 \times 48 \\ \text{Linear2: } 48 \rightarrow 2 \times 48 \\ \text{DWConv: } K=3 \times 3 \times 3, C=2 \times 48 \\ \text{SSM, } C=2 \times 48 \\ \text{Multiplicative} \\ \text{Linear3: } 2 \times 48 \rightarrow 48 \end{bmatrix} \times 3$	$\frac{D}{2} \times \frac{H}{4} \times \frac{W}{4}$
3D Conv Upsample		TransposeConv: K=2, C=32, S=2	$D \times \frac{H}{2} \times \frac{W}{2}$
Segmentation Head		Conv: K=3, C=32, S=1 Upsample: S=(1,2,2) Conv: K=1, C=Num_classes, S=1	$D \times H \times W$

Layer_name		UlikeTrans_SRA	Output Size
3D Conv Downsample		Conv: K=7, C=32, S=(1,2,2)	$D \times \frac{H}{2} \times \frac{W}{2}$
ES1	3D Conv Downsample	Conv: K=3, C=48, S=2	$\frac{D}{2} \times \frac{H}{2} \times \frac{W}{2}$
	Transformer Layer	$\begin{matrix} R = 6 \\ H = 1 \times 2 \\ E = 4 \end{matrix}$	$\frac{D}{2} \times \frac{H}{4} \times \frac{W}{4}$
ES2	3D Conv Downsample	Conv: K=3, C=128, S=2	$\frac{D}{4} \times \frac{H}{4} \times \frac{W}{8}$
	Transformer Layer	$\begin{matrix} R = 4 \\ H = 2 \times 3 \\ E = 4 \end{matrix}$	$\frac{D}{4} \times \frac{H}{8} \times \frac{W}{8}$
ES3	3D Conv Downsample	Conv: K=3, C=256, S=2	$\frac{D}{8} \times \frac{H}{16} \times \frac{W}{16}$
	Transformer Layer	$\begin{matrix} R = 2 \\ H = 4 \times 4 \\ E = 4 \end{matrix}$	$\frac{D}{8} \times \frac{H}{16} \times \frac{W}{16}$
ES4	3D Conv Downsample	Conv: K=3, C=512, S=2	$\frac{D}{16} \times \frac{H}{32} \times \frac{W}{32}$
	Transformer Layer	$\begin{matrix} R = 1 \\ H = 8 \times 3 \\ E = 4 \end{matrix}$	$\frac{D}{16} \times \frac{H}{32} \times \frac{W}{32}$
DS1	3D Conv Upsample	TransposeConv: K=2, C=256, S=2	$\frac{D}{8} \times \frac{H}{16} \times \frac{W}{16}$
	Transformer Layer	$\begin{matrix} R = 2 \\ H = 8 \times 3 \\ E = 4 \end{matrix}$	$\frac{D}{8} \times \frac{H}{16} \times \frac{W}{16}$
DS2	3D Conv Upsample	TransposeConv: K=2, C=128, S=2	$\frac{D}{4} \times \frac{H}{8} \times \frac{W}{8}$
	Transformer Layer	$\begin{matrix} R = 4 \\ H = 4 \times 4 \\ E = 4 \end{matrix}$	$\frac{D}{4} \times \frac{H}{8} \times \frac{W}{8}$
DS3	3D Conv Upsample	TransposeConv: K=2, C=48, S=2	$\frac{D}{2} \times \frac{H}{4} \times \frac{W}{4}$
	Transformer Layer	$\begin{matrix} R = 6 \\ H = 2 \times 3 \\ E = 4 \end{matrix}$	$\frac{D}{2} \times \frac{H}{4} \times \frac{W}{4}$
3D Conv Upsample		TransposeConv: K=2, C=32, S=2	$D \times \frac{H}{2} \times \frac{W}{2}$
Segmentation Head		Conv: K=3, C=32, S=1 Upsample: S=(1,2,2) Conv: K=1, C=Num_classes, S=1	$D \times H \times W$

Figure 2: **Left:** detailed configurations of UlikeMamba.3d network. Here, ‘K’: kernel size of Conv, DWConv, or TransposeConv; ‘C’: number of channels; and ‘S’: stride. **Right:** Detailed configurations of UlikeTrans.SRA network. Here, ‘R’: reduction ratio of SRA; ‘H’: head number of SRA; and ‘E’: expansion ratio of FFN.

optimizer [29] with an initial learning rate of 0.0001. All networks were trained for 1000 epochs, with each epoch consisting of 250 iterations. To evaluate the segmentation results quantitatively, we calculated the Dice coefficient (Dice), a metric measuring the overlap between the predicted segmentation and the ground truth. Additionally, we computed the floating-point operations per second (FLOPs) to assess the computational complexity of each model. Ideally, higher Dice scores indicate better segmentation accuracy, while lower FLOPs reflect greater computational efficiency.

#### 4.3. Results and Analysis

**Directly using vanilla Mamba** The results in Table 1 show that UlikeMamba.1d, using the vanilla Mamba layer with DWConv 1D, performs competitively across all datasets, achieving

Table 1: Segmentation Dice scores (higher is better) and FLOPs (lower is better) of UlikeTrans and UlikeMamba across three test datasets. ‘Parameters (Params)’ and ‘FLOPs’ are calculated based on an input size of 128×128×128 and evaluated using an NVIDIA 3090 GPU.

	AMOS	TotalSeg	BraTS	Average	Params (M)	FLOPs (G)
UlikeTrans_vanilla	OOM	OOM	OOM	OOM	31.54	OOM
UlikeTrans_SRA	88.00	79.80	90.12	85.97	45.05	64.47
UlikeMamba_1d (Vanilla)	88.40	78.00	90.20	85.53	24.10	44.88
UlikeMamba_3d	<b>89.45</b>	<b>82.60</b>	<b>90.29</b>	<b>87.45</b>	24.30	46.03

Dice scores similar to UlikeTrans\_SRA, while requiring fewer parameters and computational resources (44.88 GFLOPs vs. 64.47 GFLOPs). UlikeMamba\_1d avoids the Out of Memory (OOM) issues faced by the vanilla UlikeTrans model, which is hindered by the excessive memory demands of point-to-point self-attention for 3D volumetric data. This highlights the efficiency of Mamba in handling long-range dependencies while maintaining a low computational footprint, making it especially suited for resource-constrained environments.

The main reason is that Transformers are limited by memory capacity and complexity at higher resolutions and cannot be used directly. Moreover, when sequences are too long, establishing point-to-point relationships makes it difficult to effectively focus on key information. Mamba’s sequence modeling combined with memory modules gives it certain advantages in volume segmentation, where longer sequence modeling is required. Besides, the ability of Mamba networks to achieve comparable or even superior Dice scores to Transformer models across the datasets (AMOS, TotalSeg, BraTS) indicates their proficiency in capturing long-range spatial relationships within the data. This is particularly significant given that medical image segmentation often relies on the precise delineation of complex anatomical structures that may be distributed sparsely across the image space. The Mamba model’s performance suggests that its architecture can effectively encapsulate these relationships without the need for extensive computational resources.

**DWConv 1D vs. DWConv 3D** We noted that in vanilla Mamba layer [5] and Vision Mamba [6], DWConv 1D with a kernel size of 4 is used. However, in Mamba, the input feature embeddings are flattened and processed sequentially, causing DWConv 1D to disrupt the original 3D spatial structure. This sequential processing links distant voxels while neglecting immediate neighbors in the 3D space, undermining spatial coherence essential for accurate segmentation. To address this, we replace DWConv 1D with DWConv 3D in establishing 3D priors, ensuring local features are captured across all dimensions. This adjustment preserves the 3D structure of volumetric medical images, allowing the network to capture both local details and global context better.

As shown in Table 1, Mamba 1D performs on par with Transformer (average Dice score: Transformer 85.97 vs. Mamba 1D 85.53), while the Mamba 3D improves result from 85.53 to 87.45 and consistently outperforms Mamba 1D across all the datasets with only a slight increase in parameters and FLOPs. This proves our above claims and further demonstrates that Mamba is not only effective but also has the potential to exceed the capabilities of Transformer in volumetric medical image segmentation tasks.



## 5. Analysis 2: Mamba’s Potential in Multi-Scale Modeling

### 5.1. Experimental designs

In the first section, we establish that Mamba could effectively replace Transformers for long-range dependency modeling in volumetric medical segmentation tasks. This section aims to delve deeper into the potential of Mamba and investigate whether its long-term dependency modeling can significantly enhance multi-scale representation learning—a critical aspect of accurate volume segmentation. Multi-scale modeling plays a crucial role in medical image segmentation, where structures vary in size and capturing both fine details and broader anatomical context is essential.

While the pyramid structure captures features at different resolutions, we are further inspired by [30] to use multiple receptive fields within each resolution feature map to capture details at varying levels. Small receptive fields focus on fine structures like lesions, while larger receptive fields capture broader context, such as organ boundaries and anatomical regions. We design and implement four distinct multi-scale modeling schemes (Fig. 3). These schemes explore different strategies for fusing features from multiple receptive fields, leveraging Mamba’s and Transformer’s long-range dependency modeling capabilities for multi-scale representation learning. Specifically, we replace the whole blocks  $\mathcal{E}_i$  and  $\mathcal{D}_j$  in Eq. (1) with the following different multi-scale ones:

**MSv1** This model combines two parallel convolution layers with different kernel sizes ( $3 \times 3 \times 3$  and  $7 \times 7 \times 7$ ) to extract multi-scale features. These features are then processed through either parallel Mamba or Transformer layers. The outputs are integrated via element-wise summation, allowing efficient fusion of local and global information from different receptive fields.

**MSv2** In this configuration, the outputs from the  $3 \times 3 \times 3$  and  $7 \times 7 \times 7$  convolutions are concatenated before being processed by either Mamba or Transformer layers. This structure ensures that the multi-scale information is integrated at an earlier stage, allowing long-range dependency modeling to operate on a richer set of features.

**MSv3** This scheme extends the multi-scale feature extraction by incorporating an additional convolution layer with a  $5 \times 5 \times 5$  kernel, alongside the  $3 \times 3 \times 3$  and  $7 \times 7 \times 7$  convolutions. The outputs are concatenated and then passed through Mamba or Transformer layers. The inclusion of the intermediate  $5 \times 5 \times 5$  convolution provides an additional scale, improving the granularity of multi-scale feature extraction.

**MSv4** Designed specifically for the Mamba layer, MSv4 incorporates three DWConv 3D layers ( $3 \times 3 \times 3$ ,  $5 \times 5 \times 5$ , and  $7 \times 7 \times 7$ ) to extract multi-scale features. These are then concatenated and processed by Mamba’s state space model (SSM), which captures long-range dependencies while maintaining 3D spatial integrity. MSv4 aims to maximize Mamba’s ability to process both local and global features, taking full advantage of its sequence modeling capabilities to handle complex volumetric data efficiently.

To evaluate the effectiveness of these multi-scale modeling strategies, we systematically replace the encoder stages (ES1 to ES4) in both UlikeTrans\_SRA and UlikeMamba\_3d with the proposed MSv1, MSv2, and MSv3 schemes. MSv4, due to its specific design for Mamba, was applied only to the UlikeMamba\_3d model. This design allows us to directly compare the performance of Mamba and Transformer layers in the context of multi-scale modeling. By testing Mamba and Transformer in MSv1, MSv2, and MSv3, we can determine which architecture better exploits multi-scale features for long-range dependency modeling. Since MSv4 is specifically designed to leverage Mamba’s capabilities, it is used solely to evaluate Mamba’s efficiency in handling complex 3D medical data.

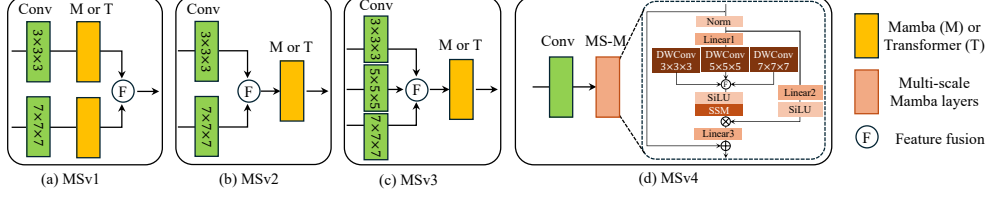


Figure 3: Four multi-scale modeling schemes for evaluating and comparing the long-range dependency modeling capabilities of Mamba and Transformers for multi-scale representation learning.

Table 2: Segmentation Dice scores (higher is better) and FLOPs (lower is better) of UlikeTrans and UlikeMamba with different multi-scale strategies across three test datasets.

	AMOS	TotalSeg	BraTS	Average	Params (M)	FLOPs (G)
UlikeTrans_SRA	88.00	79.80	90.12	85.97	45.05	64.47
UlikeTrans_SRA with MSv1	88.49 (+0.49)	82.40 (+2.60)	90.21 (+0.09)	87.03 (+1.06)	88.02	139.28
UlikeTrans_SRA with MSv2	88.87 (+0.87)	82.40 (+2.60)	90.43 (+0.31)	87.23 (+1.26)	47.83	116.59
UlikeTrans_SRA with MSv3	88.78 (+0.78)	82.70 (+2.90)	90.31 (+0.19)	87.26 (+1.29)	49.03	135.71
UlikeMamba_3d	89.45	82.60	90.29	87.45	24.30	46.03
UlikeMamba_3d with MSv1	89.43 (-0.02)	83.20 (+0.60)	90.09 (-0.20)	87.57 (+0.12)	55.13	112.50
UlikeMamba_3d with MSv2	89.33 (-0.12)	83.40 (+0.80)	90.52 (+0.23)	87.75 (+0.30)	27.09	98.16
UlikeMamba_3d with MSv3	89.50 (+0.05)	83.70 (+1.10)	90.40 (+0.11)	87.87 (+0.42)	28.29	117.28
UlikeMamba_3d with MSv4	89.48 (+0.03)	84.50 (+1.90)	90.06 (-0.23)	88.01 (+0.56)	31.57	62.23

## 5.2. Results and Analysis

The results of both UlikeTrans\_SRA and UlikeMamba\_3d architectures, incorporating different multi-scale receptive field modeling schemes, are summarized in Table 2.

**Comparison of multi-scale schemes on UlikeTrans\_SRA and UlikeMamba\_3d** Both UlikeTrans\_SRA and UlikeMamba\_3d show improvements with the application of multi-scale receptive field modeling, but UlikeMamba\_3d consistently outperforms UlikeTrans\_SRA in terms of segmentation accuracy and computational cost. For example, UlikeMamba\_3d with MSv4 achieves the highest average Dice score of 88.01 while maintaining 62.23 GFLOPs, significantly better than the 116.59 GFLOPs required by UlikeTrans\_SRA with MSv2 achieving the Dice score of 87.23.

Interestingly, the performance gains from multi-scale strategies are more noticeable in UlikeTrans\_SRA. For instance, UlikeTrans\_SRA improves from 85.97 to 87.23 with MSv2, while UlikeMamba\_3d shows a smaller improvement from 87.45 to 87.75. This may be because UlikeTrans\_SRA has lower initial performance, so it gains more from multi-scale modeling, which helps overcome self-attention’s limitations in capturing long-range dependencies in high-resolution data. In contrast, UlikeMamba\_3d is already efficient at modeling long-range dependencies through its SSM, which is well-suited for high-resolution volumetric data. As a result, Mamba-based models see relatively smaller gains from multi-scale strategies since they are already effective at capturing fine details and broader context through their long-term sequence modeling.

**Task-specific impact** The performance improvements for multi-scale schemes are most evident in the TotalSeg dataset for both UlikeTrans\_SRA and UlikeMamba\_3d. For instance, UlikeTrans\_SRA improves from 79.80 (baseline) to 82.40 (MSv2), while UlikeMamba\_3d improves from 82.60 to 84.50 with MSv4. This is in contrast to smaller gains observed on AMOS and

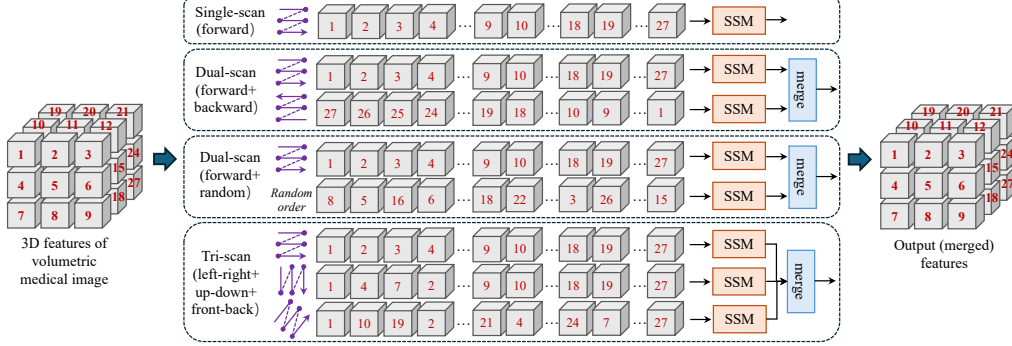


Figure 4: UlikeMamba\_3d with different sequential scanning strategies.

BraTS. The TotalSeg dataset with a larger-scale data size requires the segmentation of 117 anatomical classes, making it much more complex than AMOS (with 15 organs) and BraTS (focused on three brain tumor sub-regions). The presence of a wide range of structures in TotalSeg—varying in size from fine tissues to large anatomical structures—makes multi-scale feature extraction particularly important. The ability to capture both fine-grained and large-scale structures is crucial, and this is where the integration of multi-scale receptive fields brings significant performance improvements. In contrast, AMOS and BraTS deal with fewer segmentation classes, where a single receptive field might suffice for most features, resulting in more modest performance gains.

**Strength of MSv4** Our proposed MSv4, specifically designed for Mamba, optimizes multi-scale feature extraction in 3D medical data. It delivers the best overall performance across datasets while maintaining lower computational costs. With MSv4, UlikeMamba\_3d achieves the highest Dice score on TotalSeg (84.50) and remains competitive on AMOS and BraTS, all with fewer FLOPs than other multi-scale schemes. MSv4’s design excels by fully leveraging Mamba’s SSM for efficient long-range dependency modeling, integrating multi-scale features with minimal overhead, making it ideal for complex volumetric segmentation tasks.

## 6. Analysis 3: Multi-scan Strategy vs Single-scan Strategy

### 6.1. Experimental designs

Mamba’s core mechanism, particularly its parallelized selective scan operation, was originally designed for one-dimensional sequential data processing. This introduces potential challenges when adapting it to visual data, where spatial components are not inherently sequential. To address this, Vision Mamba [6] and Vmamba [7] propose multi-way scanning mechanisms tailored to preserve spatial coherence in vision tasks. The goal here is to assess whether these complex scanning strategies are needed or if simpler approaches suffice for volumetric medical image segmentation, where maintaining spatial relationships between voxels is critical for accuracy.

To investigate, we conducted experiments using the same backbone architecture UlikeMamba\_3d but varied the scanning mechanism to evaluate its effect on segmentation performance. In other words, we consider different scanning strategies for UlikeMamba\_3d by modifying it in  $h$  of Eq. (1) only. We implemented the following scanning strategies, as shown in Fig. 4: **Single-scan** [5], proposed in vanilla Mamba, processes 3D features by flattening the

volumetric features and scanning them sequentially along a single axis, typically in the forward direction. **Dual-scan (forward + backward)**, proposed in Vision Mamba [6], processes 3D input by scanning twice along the same axis—once in the forward direction and once in the backward direction. The features from both scans are then merged, allowing the model to incorporate information from both directions along the chosen axis. This method maintains the same backbone structure but introduces bidirectional data flow in Mamba layers to capture more comprehensive spatial information. **Dual-scan (forward + random)** is a new approach that combines a standard forward scan with an additional scan in random order. This method introduces variation in the scanning sequence to capture a broader range of spatial relationships while still preserving the overall sequential structure. The features from forward and random scans are merged to create a more diverse feature representation of the volumetric input. **Tri-scan**, inspired by Vmamba [7] and adapted for 3D medical volumetric data, scans the input in three directions: left-right, up-down, and front-back. Each scan generates a sequence of features along its respective axis. These features are then passed through separate SSM layers for further processing, and the outputs are merged to form a unified representation of the 3D volume.

## 6.2. Results and Analysis

**Results** The experimental results are summarized in Table 3. Across the three datasets (AMOS, TotalSeg, and BraTS), we observe that Tri-scan achieves the highest average Dice score (87.93) but comes at the cost of increased computational complexity, as indicated by its higher parameter count (26.38M) and FLOPs (53.09G). The dual-scan (forward + backward) approach performs slightly better than the single-scan and dual-scan (forward + random) approaches, with an average Dice score of 87.67 and 87.60, respectively. However, the performance gains for dual-scan methods over single-scan are marginal. While having the lowest computational requirements (24.30M parameters, 46.03G FLOPs), the Single-scan method still delivers competitive performance with an average Dice score of 87.45, closely trailing the more complex scanning mechanisms.

**Analysis** The Dual-scan (forward + backward) method aims to help the model capture spatial information from both the start and end of the sequence, potentially building a more complete data representation. However, in our task, the improvement over the Single-scan is slight, probably because 3D medical images have strong structural priors, allowing most key spatial relationships to be captured effectively by a unidirectional scan. The added backward scan introduces limited sequential diversity, failing to uncover significantly more data patterns. Besides, Mamba’s long-range dependency modeling is already highly effective, further reducing the need for a backward pass. As a result, the additional computational cost of the backward scan brings little benefit, resulting in only slight gains in segmentation accuracy.

The Dual-scan (forward + random) method, which introduces a random scan alongside a forward pass, is designed to capture more complex sequential relationships that may not be evident in standard scanning orders.

Although randomizing the scanning order can diversify the captured spatial relationships, it also risks compromising the spatial coherence of the data, which could explain why its performance is on par with Dual-scan (forward + backward) rather than exceeding it. This method may identify some complex dependencies but does so at the cost of distorting the structural priors of medical images, which is essential for precise segmentation.

Tri-scan obtains the best results, achieving the highest Dice scores across all datasets. Scanning in three directions (left-right, up-down, front-back) effectively mitigates the spatial discontinuity that can arise from sequential scanning, ensuring a more thorough capture of spatial

Table 3: Segmentation Dice scores (higher is better) and FLOPs (lower is better) of UlikeMamba with different sequential modeling scanning strategies across three test datasets.

	AMOS	TotalSeg	BraTS	Average	Params (M)	FLOPs (G)
Single-scan	89.45	82.60	90.29	87.45	24.30	46.03
Dual-scan (forward + backward)	89.74 (+0.29)	83.00 (+0.40)	90.27 (-0.02)	87.67 (+0.22)	25.34	49.56
Dual-scan (forward + random)	89.42 (-0.03)	83.30 (+0.70)	90.08 (-0.21)	87.60 (+0.15)	25.34	49.56
Tri-scan	89.77 (+0.32)	83.60 (+1.00)	90.43 (+0.14)	87.93 (+0.48)	26.38	53.09

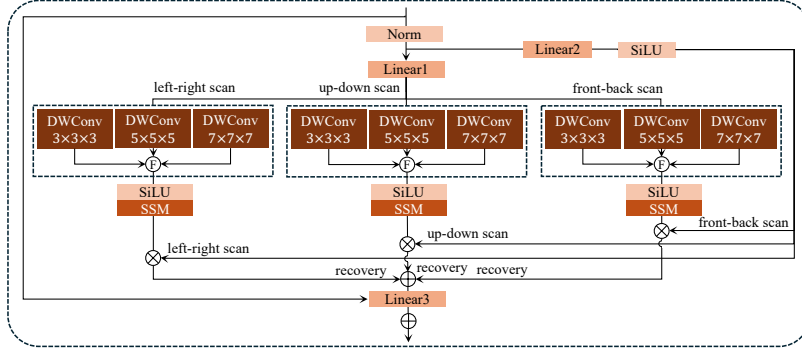


Figure 5: Our proposed Mamba layer in UlikeMamba\_3dMT, which modifies the original 1D depthwise convolution to 3D depthwise convolution, embraces a multi-scale strategy and incorporates tri-directional scanning to capture comprehensive spatial relationships in 3D volumetric data more effectively.

relationships across the 3D volume. This is particularly beneficial for tasks like TotalSeg, where the segmentation involves 117 classes and complex spatial relationships are needed to be captured. The improvement in TotalSeg is more pronounced since the complexity of the task, which requires distinguishing between a wide variety of structures, benefits more from a comprehensive multi-directional scan. Despite this, the trade-off is clear—the higher computational cost makes Tri-scan limitations for resource-constrained applications.

## 7. Comparison with Advanced Baselines

To further validate the correctness of the aforementioned conclusions, we integrate all the validated strategies into a unified model and compare its performance against advanced baselines. Specifically, we 1) replace the Transformer with Mamba while modifying the 1D depthwise convolution to 3D depthwise convolution in the Mamba layer, 2) adopt the multi-scale strategy, *i.e.*, MSv4, and 3) adopt tri-directional scanning, *i.e.*, Tri-scan, to better capture comprehensive spatial relationships in 3D volumetric data. We denote this network as UlikeMamba\_3dMT. The specific architecture details of the Mamba layer in UlikeMamba\_3dMT can be found in Fig. 5.

The results in Fig. 6 demonstrate the superiority of UlikeMamba\_3dMT over other advanced networks on both AMOS and BraTS datasets. UlikeMamba\_3dMT achieves the competitive Dice scores (89.95 in AMOS and 90.60 in BraTS) with the lowest computational cost (93.09G FLOPs), outperforming leading the CNN-based network nnUNet [3], Transformer-based net-

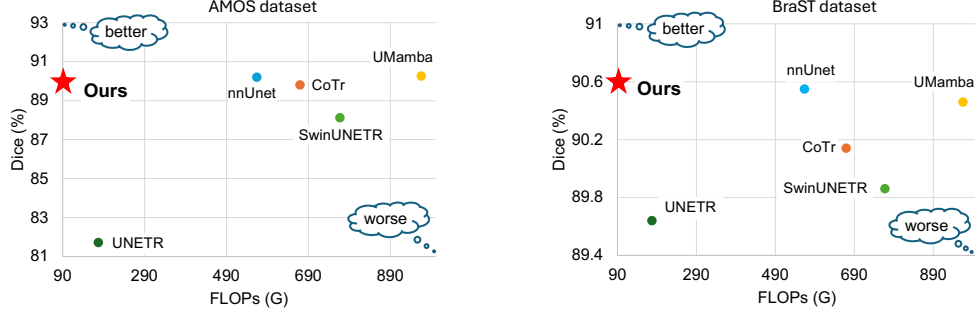


Figure 6: Segmentation Dice scores (higher is better) and FLOPs (lower is better) of UlikeMamba\_3dMT and against advanced baselines on AMOS and BraTS test sets.

works such as CoTr [31], UNETR [32], and SwinUNETR [33], as well as the existing Mamba-based networks U-Mamba [8], which simply integrates Mamba with CNNs.

Our UlikeMamba\_3dMT integrates Mamba’s SSM with 3D depthwise convolutions, the proposed multi-scale modeling, and the designed Tri-scan strategy, proving highly effective by delivering competitive accuracy (Dice scores) while maintaining computational efficiency. This establishes UlikeMamba\_3dMT as a new benchmark in 3D medical image segmentation.

## 8. Conclusion and Future Work

In this study, we present a comprehensive analysis of the Mamba architecture for 3D medical image segmentation, thoroughly investigating three critical aspects: its viability as an alternative to Transformers, its ability to enhance multi-scale representation learning, and the necessity of complex scanning strategies. Our evaluation across diverse and challenging benchmarks - AMOS, TotalSegmentator, and BraTS - demonstrates several key strengths of Mamba. Specifically, Mamba provides a computationally efficient and effective alternative to Transformers, excelling particularly when augmented with custom-designed 3D depthwise convolutions. This leads to improved segmentation accuracy while significantly reducing computational requirements, benefiting tasks with extensive volumetric data or limited computational resources.

Furthermore, our multi-scale Mamba block (MSv4) effectively captures both fine-grained details and global contextual information. This capability is particularly important in complex segmentation tasks like those presented in segmenting 117 anatomical structures, where multiple anatomical structures of varying sizes must be accurately delineated.

Beyond architecture design, our study critically assesses scanning strategies, demonstrating that while simpler approach such as single-scan is adequate for many applications, the Tri-scan approach significantly enhances performance in highly challenging cases by better capturing comprehensive spatial relationships across all dimensions of 3D data.

Our proposed UlikeMamba\_3dMT network, which integrates all these validated strategies: 3D depthwise convolutions, multi-scale modeling, and Tri-scan, establishes a new benchmark for 3D medical image segmentation. It outperforms advanced models such as nnUnet, CoTr, UNETR, SwinUNETR, and U-Mamba, achieving competitive Dice scores with reduced computational complexity.

However, our study has several limitations. First, our validation of Mamba’s effectiveness compared to Transformers relies mainly on empirical results, lacking analytical insights supported by mathematical derivation. A deeper theoretical exploration could offer more founda-

tional understanding regarding Mamba’s superior performance. Besides, the current Mamba-based architecture still integrates convolutional kernels to handle volumetric data. Future research could aim to develop a fully convolution-free, pure Mamba-based architecture tailored explicitly for high-resolution 3D medical image segmentation, potentially further enhancing computational efficiency and segmentation accuracy.

### Declaration of generative AI and AI-assisted technologies in the writing process

During the preparation of this work the author(s) used GPT-4o in order to improve language and readability. After using this tool/service, the author(s) reviewed and edited the content as needed and take(s) full responsibility for the content of the publication.

### References

- [1] O. Ronneberger, P. Fischer, T. Brox, U-net: Convolutional networks for biomedical image segmentation, in: International Conference on Medical image computing and computer-assisted intervention, Springer, 2015, pp. 234–241.
- [2] Z. Zhou, M. M. R. Siddiquee, N. Tajbakhsh, J. Liang, Unet++: Redesigning skip connections to exploit multiscale features in image segmentation, *IEEE Transactions on Medical Imaging* 39 (6) (2019) 1856–1867.
- [3] F. Isensee, P. F. Jaeger, S. A. Kohl, J. Petersen, K. H. Maier-Hein, nnu-net: a self-configuring method for deep learning-based biomedical image segmentation, *Nature methods* 18 (2) (2021) 203–211.
- [4] A. Vaswani, N. Shazeer, N. Parmar, J. Uszkoreit, L. Jones, A. N. Gomez, Ł. Kaiser, I. Polosukhin, Attention is all you need, in: Proceedings of the 31st International Conference on Neural Information Processing Systems, 2017, pp. 6000–6010.
- [5] A. Gu, T. Dao, Mamba: Linear-time sequence modeling with selective state spaces, *arXiv preprint arXiv:2312.00752* (2023).
- [6] L. Zhu, B. Liao, Q. Zhang, X. Wang, W. Liu, X. Wang, Vision mamba: Efficient visual representation learning with bidirectional state space model, in: Forty-first International Conference on Machine Learning, 2024, pp. –.
- [7] Y. Liu, Y. Tian, Y. Zhao, H. Yu, L. Xie, Y. Wang, Q. Ye, J. Jiao, Y. Liu, Vmamba: Visual state space model, *Advances in neural information processing systems* 37 (2024) 103031–103063.
- [8] J. Ma, F. Li, B. Wang, U-mamba: Enhancing long-range dependency for biomedical image segmentation, *arXiv preprint arXiv:2401.04722* (2024).
- [9] Z. Xing, T. Ye, Y. Yang, G. Liu, L. Zhu, Segmamba: Long-range sequential modeling mamba for 3d medical image segmentation, in: proceedings of Medical Image Computing and Computer Assisted Intervention – MICCAI 2024, 2024, pp. 578 – 588.
- [10] J. Liu, H. Yang, H.-Y. Zhou, Y. Xi, L. Yu, C. Li, Y. Liang, G. Shi, Y. Yu, S. Zhang, H. Zheng, S. Wang, Swin-umamba: Mamba-based unet with imagenet-based pretraining, in: proceedings of Medical Image Computing and Computer Assisted Intervention – MICCAI 2024, 2024, pp. 615 – 625.
- [11] Q. Lin, Z. Li, K. Zeng, J. Wen, Y. Jiang, J. Chen, Wtngan: Unpaired image translation from white light images to narrow-band images, *Pattern Recognition* (2025) 111431.
- [12] Y. Ji, H. Bai, C. Ge, J. Yang, Y. Zhu, R. Zhang, Z. Li, L. Zhanng, W. Ma, X. Wan, et al., Amos: A large-scale abdominal multi-organ benchmark for versatile medical image segmentation, *Advances in neural information processing systems* 35 (2022) 36722–36732.
- [13] J. Wasserthal, H.-C. Breit, M. T. Meyer, M. Pradella, D. Hinck, A. W. Sauter, T. Heye, D. T. Boll, J. Cyriac, S. Yang, et al., Totalsegmentator: robust segmentation of 104 anatomic structures in ct images, *Radiology: Artificial Intelligence* 5 (5) (2023).
- [14] U. Baid, S. Ghodasara, S. Mohan, M. Bilello, E. Calabrese, E. Colak, K. Farahani, J. Kalpathy-Cramer, F. C. Kitamura, S. Pati, et al., The rsna-asnr-miccai brats 2021 benchmark on brain tumor segmentation and radiogenomic classification, *arXiv preprint arXiv:2107.02314* (2021).
- [15] F. Chollet, Xception: Deep learning with depthwise separable convolutions, in: Proceedings of the IEEE conference on computer vision and pattern recognition, 2017, pp. 1251–1258.
- [16] J. Chen, J. Mei, X. Li, Y. Lu, Q. Yu, Q. Wei, X. Luo, Y. Xie, E. Adeli, Y. Wang, et al., Transunet: Rethinking the unet architecture design for medical image segmentation through the lens of transformers, *Medical Image Analysis* (2024) 103280.

- [17] Q. Yan, S. Liu, S. Xu, C. Dong, Z. Li, J. Q. Shi, Y. Zhang, D. Dai, 3d medical image segmentation using parallel transformers, *Pattern Recognition* 138 (2023) 109432.
- [18] X. Guo, X. Lin, X. Yang, L. Yu, K.-T. Cheng, Z. Yan, Uctnet: Uncertainty-guided cnn-transformer hybrid networks for medical image segmentation, *Pattern Recognition* 152 (2024) 110491.
- [19] C. Huang, Z. Wu, H. Xi, J. Zhu, kmaxu: Medical image segmentation u-net with k-means mask transformer and contrastive cluster assignment, *Pattern Recognition* 161 (2025) 111274.
- [20] J. Wang, J. Chen, D. Z. Chen, J. Wu, Lkm-unet: Large kernel vision mamba unet for medical image segmentation, in: *proceedings of Medical Image Computing and Computer Assisted Intervention – MICCAI 2024*, Vol. LNCS 15008, Springer Nature Switzerland, 2024, pp. 360 – 370.
- [21] Z. Xu, F. Tang, Z. Chen, Z. Zhou, W. Wu, Y. Yang, Y. Liang, J. Jiang, X. Cai, J. Su, Polyp-mamba: Polyp segmentation with visual mamba, in: *proceedings of Medical Image Computing and Computer Assisted Intervention – MICCAI 2024*, 2024, pp. 510 – 521.
- [22] R. Wu, Y. Liu, P. Liang, Q. Chang, H-vmunet: High-order vision mamba unet for medical image segmentation, *Neurocomputing* (2025) 129447.
- [23] A. Chang, J. Zeng, R. Huang, D. Ni, Em-net: Efficient channel and frequency learning with mamba for 3d medical image segmentation, in: *proceedings of Medical Image Computing and Computer Assisted Intervention – MICCAI 2024*, Vol. LNCS 15009, Springer Nature Switzerland, 2024, pp. 266 – 275.
- [24] H. Wang, Y. Lin, X. Ding, X. Li, Tri-plane mamba: Efficiently adapting segment anything model for 3d medical images, in: *proceedings of Medical Image Computing and Computer Assisted Intervention – MICCAI 2024*, Vol. LNCS 15009, Springer Nature Switzerland, 2024, pp. 636 – 646.
- [25] M. Zhang, Y. Yu, S. Jin, L. Gu, T. Ling, X. Tao, Vm-unet-v2: rethinking vision mamba unet for medical image segmentation, in: *International Symposium on Bioinformatics Research and Applications*, Springer, 2024, pp. 335–346.
- [26] W. Zhao, F. Wang, Y. Wang, Y. Xie, Q. Wu, Y. Zhou, Ud-mamba: A pixel-level uncertainty-driven mamba model for medical image segmentation, *arXiv preprint arXiv:2502.02024* (2025).
- [27] C. Ma, Z. Wang, Semi-mamba-unet: Pixel-level contrastive and cross-supervised visual mamba-based unet for semi-supervised medical image segmentation, *Knowledge-Based Systems* 300 (2024) 112203.
- [28] W. Wang, E. Xie, X. Li, D.-P. Fan, K. Song, D. Liang, T. Lu, P. Luo, L. Shao, Pyramid vision transformer: A versatile backbone for dense prediction without convolutions, in: *Proceedings of the IEEE/CVF international conference on computer vision*, 2021, pp. 568–578.
- [29] I. Loshchilov, F. Hutter, Decoupled weight decay regularization, in: *International Conference on Learning Representations*, 2019, pp. –.
- [30] C. Szegedy, W. Liu, Y. Jia, P. Sermanet, S. Reed, D. Anguelov, D. Erhan, V. Vanhoucke, A. Rabinovich, Going deeper with convolutions, in: *Proceedings of the IEEE conference on computer vision and pattern recognition*, 2015, pp. 1–9.
- [31] Y. Xie, J. Zhang, C. Shen, Y. Xia, Cotr: Efficiently bridging cnn and transformer for 3d medical image segmentation, in: *Medical Image Computing and Computer Assisted Intervention–MICCAI 2021: 24th International Conference*, Strasbourg, France, September 27–October 1, 2021, *Proceedings, Part III* 24, Springer, 2021, pp. 171–180.
- [32] A. Hatamizadeh, Y. Tang, V. Nath, D. Yang, A. Myronenko, B. Landman, H. R. Roth, D. Xu, Unetr: Transformers for 3d medical image segmentation, in: *Proceedings of the IEEE/CVF winter conference on applications of computer vision*, 2022, pp. 574–584.
- [33] A. Hatamizadeh, V. Nath, Y. Tang, D. Yang, H. R. Roth, D. Xu, Swin unetr: Swin transformers for semantic segmentation of brain tumors in mri images, in: *International MICCAI brainlesion workshop*, Springer, 2021, pp. 272–284.